# Geometric and electronic structure of graphene bilayer edges

Ji Feng,[1] Liang Qi,[1] Jian Yu Huang,[2] and Ju Li[1,*]
[1]*Department of Materials Science and Engineering, University of Pennsylvania, Philadelphia, Pennsylvania 19104, USA*
[2]*Center for Integrated Nanotechnologies, Sandia National Laboratories, Albuquerque, New Mexico 87185, USA*
(Received 2 September 2009; published 9 October 2009)

We present a computational investigation of free-standing graphene bilayer edge (BLE) structures, aka "*fractional nanotubes*." We demonstrate that these curved carbon nanostructures possess a number of interesting properties, electronic in origin. The BLEs, quite atypical of elemental carbon, have large permanent electric dipoles of 0.87 and 1.14 debye/Å for zigzag and armchair inclinations, respectively. An unusual, weak *AA* interlayer coupling leads to a twinned double-cone dispersion of the electronic states near the Dirac points. This entails a type of quantum Hall behavior markedly different from what has been observed in graphene-based materials, characterized by a magnetic field-dependent resonance in the Hall conductivity.

DOI: 10.1103/PhysRevB.80.165407 PACS number(s): 73.22.−f, 73.43.−f, 81.05.Uw, 81.05.Zx

Free-standing graphene monolayers (GMLs) (Ref. 1) have attracted tremendous interest owing to a variety of exotic electronic properties, including in particular integer quantum Hall effects (QHEs), as a consenquence of a Berry phase of $\pi$.[1–5] An ideal infinite GML's $p_z p_z \pi$ energy spectrum is characterized by being gapless, with a cone-shaped dispersion around the Fermi level, at the vertices ($K$ and $K'$, often referred to as Dirac points for graphene) of the first Brillouin zone (1BZ). This linear dispersion leads to a Fermi velocity of $v_F \sim 10^6$ m/s and a vanishingly small effective mass for low-energy excitations. Graphene bilayers with *AB* stacking have also been prepared. Graphene and *AB*-stacked graphene bilayer show two types quantum Hall conductivity stairs.[6] In the *AB* bilayer, there is a $2\pi$ Berry phase and zero-level anomaly in QHE conductivity[6,7] because of a weak interlayer interaction.[6,8] The zero-level anomaly is not seen in the GMLs.

A novel form of graphene nanostructure was recently discovered,[9] which can be viewed as two flat graphene layers continuously connected by a curved bilayer edge (BLE, see Fig. 1). Geometrically, a BLE can be considered a "fractional nanotube."[10,11] Detailed transmission electron microscopy (TEM) revealed that in these BLE structures the flat bilayer regions are forced into *AA* stacking,[10] a geometry that is not usually seen. Lammert *et al.*[12] have studied theoretically the electronic structure of "squashed nanotubes," where the electronic structure is sensitive to the interlayer coupling. Here we investigate the geometric and electronic structures of graphene BLEs using a combination of density-functional theory[13] (DFT) and tight-binding (TB) methods. We show that these BLE structures have extensive permanent electric dipoles. Our analysis of the electronic structure also indicates that the BLE structures will show a type of QHE, characterized by magnetic field-dependent anomalous resonance between two separate QHE sequences as the doping level is continuously varied, which is markedly different from QHE previously observed in graphene.[6]

*In situ* TEM observations of Joule-heated few-layer graphene reveal that graphene monolayer edges (MLEs) are atomically rough and not strongly faceted crystallographically.[11,14] In contrast, when two MLEs react to form a more stable BLE, the newly formed BLE tends to be atomically sharp and strongly faceted into zigzag and armchair inclinations.[11,14] This suggests that in the Wulff plot[15] of edge energy versus inclination angle, zigzag and armchair inclinations are strongly favored in the BLE Wulff plot, whereas it is not the case in the MLE Wulff plot. Consequently, we propose that there is a geometrical reason for this strong preference of zigzag and armchair inclined BLEs. Unlike rolling carbon nanotubes which involves 360° rotation of graphene, rolling graphene into a BLE requires 180° rotation only (see Fig. 1). Generally speaking the lattice orientation of the top and bottom graphene layers can differ, like what happens when one folds a piece of ruled writing-pad paper along an arbitrary crease line. Yet, there is an *orientation constraint*, enforced through the common preparation

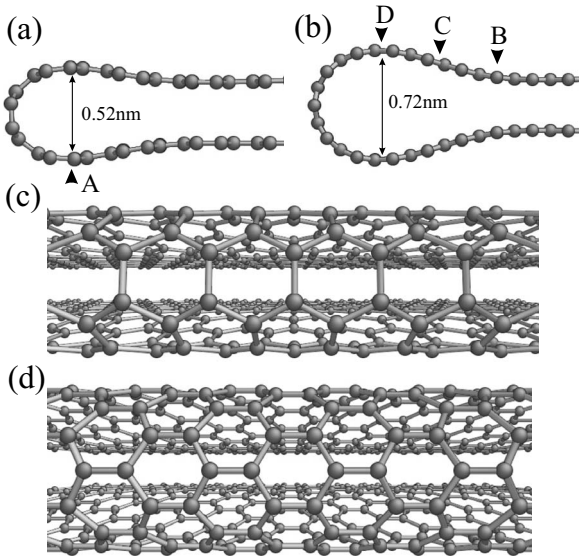


FIG. 1. The atomic structures of bilayer edges from DFT-LDA optimization. (a) and (b) show sideviews (normal projections along the edge direction) of the zigzag and armchair bilayer edges, respectively. (c) and (d) are closeup perspective views of the zigzag and armchair bilayer edges. We call these BLEs *zigzag* or *armchair* based on the orientation of $C_6$ hexagon along the edge. As we see in (c), in zigzag BLE a hexagon has two sides perpendicular to the edge direction while in armchair BLE in (d) a hexagon has two sides parallel to the edge. Both BLEs shown lead to *AA* stacking of the two graphene layers in the flat regions.

 

procedures of BLEs,[10,11] that the top and bottom graphene sheets must have identical or symmetry-operation equivalent lattice orientations. The only ways this orientation constraint can be satisfied without disrupting the hexagonal C-C bonding network are by folding along one of the six *mirror axes* (or the $C_2'$ and $C_2''$ axes of the $D_{6h}$ point group) of the graphene lattice: the three armchair or the three zigzag inclinations. Creating BLEs along any other inclinations under the common orientation constraint would require two simultaneous processes. First one is the elastic folding of the graphene, which is a low-energy process. The other process is the introduction of high-energy topological defects such as pentagon and/or heptagon that would disrupt the covalent bonding network.[14] (Pentagons/heptagons are needed to compensate for the orientation change due to elastic folding, like dislocations in a grain boundary.[16])

Thus, the BLE Wulff plot must have very deep energy cusps for zigzag and armchair inclinations under the common orientation constraint while the MLE Wulff plot should be more isotropic.[14] In this sense, the inclination preference of BLEs are quite different from carbon nanotubes, which admit all kinds of chiral folding angles in a low-energy elastic folding process. In addition, one should be aware of the terminology that because we use graphene inclination rather than axial direction to label BLEs, a zigzag BLE is really a "fractional armchair nanotube" [Figs. 1(a) and 1(c)] and an armchair BLE is a "fractional zigzag nanotube" [Figs. 1(b) and 1(d)]. In this paper, we will focus on only the zigzag and armchair BLEs under the common orientation constraint.

In contrast to MLEs which even after reconstruction have dangling bonds and/or pentagons or heptagons,[17] zigzag and armchair BLEs have exceptional energetic stability similar to carbon nanotubes due to low-energy folding. But unlike circular carbon nanotubes which admits a range of elastic folding radius, the BLEs are highly monodisperse atomic structures, with folding curvature controlled by a competition/compromise between van der Waals adhesion and elastic bending energy. The bending energy $E_{\text{bending}}=\int_{\Sigma} ds \lambda R(s)^{-2} \propto \lambda/\bar{R}$ (where $\lambda$ is the bending modulus), which is positive, favors a large radius of curvature $\bar{R}$; whereas van der Waals adhesion energy between the top and bottom layers, which is negative, favors a small radius of curvature $\bar{R}$, in order to maximize the stabilizing adhesion in the flat area. As shown in Fig. 1, this competition results in an optimal radius of curvature for zigzag and armchair BLE, respectively.

There is also a "rolling tank tread" degree of freedom with zigzag and armchair BLEs. This corresponds to a motion in which the top and bottom sheets translate in opposite directions (perpendicularly to the edge) by $\mathbf{d}/2$ in plane without changing lattice orientations.[12] The change in edge energy in reference to the *AA* state, $E_{\text{BLE}}(\mathbf{d})-E_{\text{BLE}}(AA)$, is expected to be rather small for such perpendicular $\mathbf{d}$ shifts, corresponding to soft "tank treading" degree of freedom. If however the in-plane shift $\mathbf{d}$ is *parallel* to the edge, one expects $E_{\text{BLE}}(\mathbf{d})-E_{\text{BLE}}(AA)$ to increase dramatically because in-plane shearing of the C-C bonding network would be required. It is then easy to see that while *AB* stacking is compatible with zigzag BLE (because *AB*-zigzag BLE can be produced from *AA*-zigzag BLE by soft tank treading), *AB* stacking is geometrically incompatible with armchair BLE, with $E_{\text{armchair BLE}}(AB) \gg E_{\text{armchair BLE}}(AA)$. This may explain why in the experiment, *AA* instead of *AB* stacking was found[10] because although *AB* stacking leads to reasonably low zigzag BLE energy, it leads to too high armchair BLE energy. *AA* stacking leads to reasonably low edge energy for both zigzag and armchair BLEs, having the highest symmetry among all $\mathbf{d}$ translations. Armchair BLEs were indeed found in Liu *et al.*'s[10] high-resolution TEM experiment.

The relative stability of a bilayer graphene flake that is *AB* stacked versus *AA* stacked is therefore modeled as $\Delta E_{\text{total}}=[E_{\text{BLE}}(AB)-E_{\text{BLE}}(AA)]l+[\gamma(AB)-\gamma(AA)]A$, where $l$ is the flake circumference, $A$ is the flake area, $\gamma(AB)$ and $\gamma(AA)$ are the adhesion energy per unit area for *AB*- and *AA*-stacked flat bilayer graphene, respectively. We know the first term is positive from our calculations and the second term is negative since a large enough bilayer flake would prefer *AB* stacking.[6] Thus, the model predicts there is a critical size, above which *AB* stacking is preferred in the center region of the flake, below which *AA* stacking is preferred throughout. In the present work we will focus on analyzing *AA*-stacked zigzag and armchair BLEs.[10]

Current implementation of DFT generally cannot accurately capture the long-range electron correlations responsible for van der Waals adhesion. In the case of graphite and related structures, however, the local-density approximation (LDA) (Refs. 13 and 18) can yield an adequate level of accuracy describing the equilibrium interaction potential between graphite layers.[19] We therefore employ the DFT-LDA method with a plane-wave basis set as implemented in Vienna *ab initio* simulation package.[20] Only the four outer electrons of carbon enter the self-consistent fields in the optimization of electronic degrees of freedom while the nuclei and 1*s* electrons are embedded in the ultrasoft pseudopotential[21] constructed with the projector augmented-wave method.[22,23]

It is noted that in the LDA-optimized zigzag BLE (Fig. 1), the maximum top-bottom separation in the edge region is around 0.52 nm. In the flat region the layer separation is around 0.36 nm, close to the van der Waals separation between adjacent layers in graphite. For armchair BLE the separation in the edge region is around 0.72 nm and that of the flat region is 0.37 nm. We see that the interlayer spacing outside the edge region is within the attractive regime of the van der Waals potential.[19] This supports the idea that the binding force in the flat region is important for the special geometry of the BLEs. The thicknesses at the edge of a BLE is connected to the bending modulus (flexural rigidity) of the graphene sheet. The fact that this value is significantly different for zigzag and armchair configurations reflects the anisotropy in large bending of graphene sheet.[24] Therefore, the armchair BLE forms larger bulge to lower overall radius of curvature, given the bending energy $E_{\text{bending}}=\int_{\Sigma} ds \lambda R(s)^{-2}$ (where $\lambda$ is the bending modulus). The C-C bond lengths, $b$, in the LDA-optimized geometry generally increase from 1.41 Å in the flat region to 1.42 Å into the edge region.

One may intuitively view BLE as a *fractional nanotube*.[11] It has been pointed out that in conventional circular carbon nanotubes, even though the overall dipole moment is absent for symmetry reasons, there is still curvature-induced polarization on individual atoms,[25] which cancels out when all

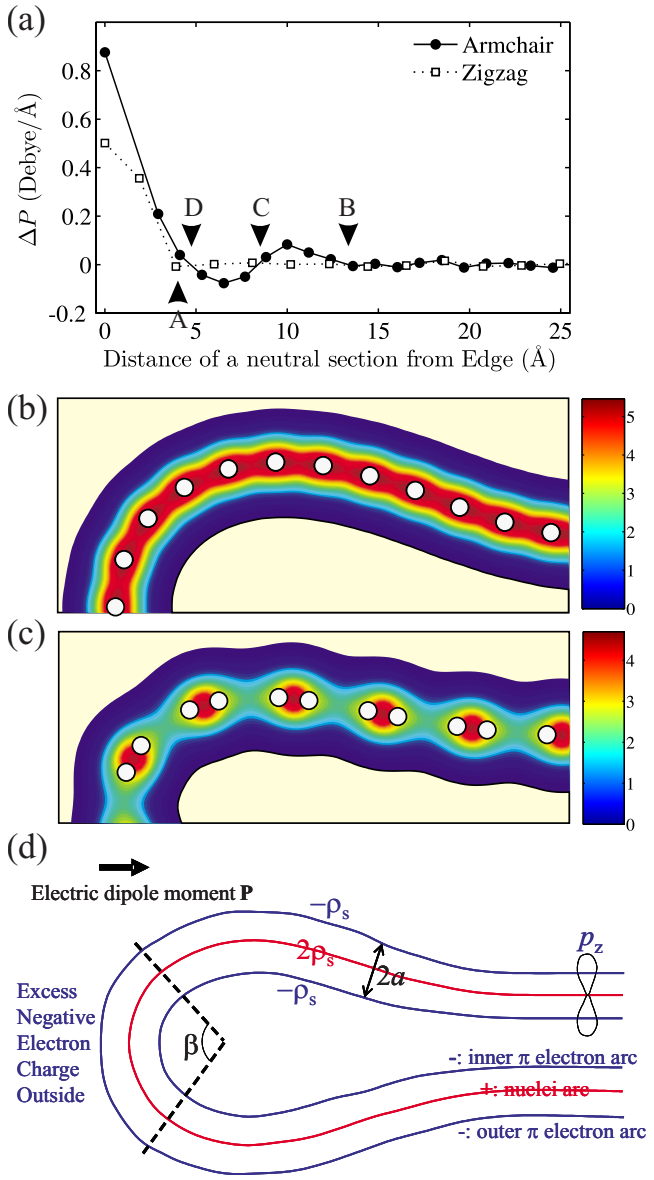


FIG. 2. (Color online) Extensive dipolar BLEs. (a) Dipole moments of electrically neutral slices of the BLEs. Each half of the unit cell (left or right) is electrically neutral. We subsequently find successive vertical planes, between which electrical neutrality is satisfied. The local dipole moment density (averaged over the width of the unit cell along the longitudinal direction), $\Delta P$ (debye/Å), is calculated for each of the neutral slices. Valence electron density of (b) armchair and (c) zigzag bilayer edges, respectively. The values plotted are the integration along the longitudinal (out-of-plane) direction in a unit cell. Scale bar units: e/Å$^2$. (d) A simple triple-arc model describing the charge distribution in the BLE. Blue and red lines represent the continuous distribution of negative and positive charges, respectively. Overall charge neutrality is maintained in this model.

atoms are summed. But since a fractional nanotube obviously lacks left-right and/or rotational symmetry, a net permanent dipole moment $\mathbf{P} \equiv \int_\Omega d^3\mathbf{x}\rho(\mathbf{x})\mathbf{x}$ is admissible, which can be obtained from the DFT charge densities [Figs. 2(b) and 2(c)]. To estimate the sign and magnitude of BLE electric dipole **P**, we devise a simple "triple-arc" geometrical model, Fig. 2(d), to facilitate a back-of-envelope prediction. In this model the positive charges are distributed uniformly along a central arc to mimic the positively charged ions. The negative charges from the $\pi$ electrons are assumed to be uniformly distributed along two (outer and inner) arcs sandwiching and at equal distances $a$ from the central arc. This cartoon is motivated by the observation that $p_z p_z \pi$ density has node at the center and is maximized at a finite distance ($\sim a$) away from the center on top (outer arc) and bottom (inner arc), respectively. For flat graphene, the outer, central, and inner arcs are equally long and the negative charge is equally split between the outer and inner arcs, which leads to zero dipole. However, when graphene is bent to form BLE, the outer arc becomes longer than the inner arc. We further assume that the negative charge density (charge per arc length) $\rho_s$ stays equal between the outer and inner arcs, upon bending. This assumption has been roughly validated by inspecting the DFT charge densities [Figs. 2(b) and 2(c)]. If the negative charge per arc length is equal, but the outer arc is longer than the inner arc, there must be a net transfer of electron from the inside to the outside of BLE, i.e., there is a net displacement of negative charge center toward the outside, establishing a net dipole moment **P** pointing inward, shown in Fig. 2(d). For a rough estimate, we assume the negative charge transfer comes entirely from the distal end of the edge subtended by angle $\beta$, shown in Fig. 2(d). We also ignore contributions from the rest of the system: $\Delta Q = e(R+a)\beta\rho_s - e(R-a)\beta\rho_s = 2ea\beta\rho_s$, where $R$ is the radius of curvature. $\rho_s \approx \rho_s^0$, the $\pi$ electron density per arc length for flat graphene since to leading order in bending curvature the sum of outer and inner arc lengths equals twice the central arc length, unchanged from the flat state. $\rho_s$ can thus be estimated, given there is one $p_z$ electron per atom. And then $P = \frac{\sin(\beta/2)}{\beta/2}\Delta Q a = 4ea^2\rho_s \sin(\beta/2)$. Taking $a = 0.7$ Å (half C-C bond length) and $\beta = \pi/2$, we obtain an estimate of BLE dipole to be $\sim 1.3$ debye/Å.

To unambiguously determine the dipole moment of the BLEs from DFT ground-state density, we calculated the local dipoles of electrically neutral sections of the model structure, as shown in Fig. 2(a). To obtain the electrically neutral sections of the model structure, we begin with a plane outside the distal end of the BLE and search for the location of the next parallel plane, such that the two planes sandwich a region where the charges of valence electrons and ion cores in this region cancel. Successive neutral sections are similarly located. Subsequently, the dipole moment of each individual neutral section was computed. Because the planes found by this algorithm are so densely packed close to the edge, their spacing is on the order of the real-space Fourier grid spacing. For this reason, a few neutral sections close to the edge are grouped into one large section and the total dipole moment is calculated and the location of the grouped large section is taken to be 0 (i.e., right at the edge).

We see that in the flat regions, the local dipole moment is very small with minor spatial fluctuations, for both armchair and zigzag BLEs. But as we move into the BLE region, the dipole moment attains considerable magnitude and is remarkably sensitive to local curvature. When a graphene sheet is bent, we expect the *unrelaxed* electronic density to have a higher Hartree energy density along the side toward the cen-

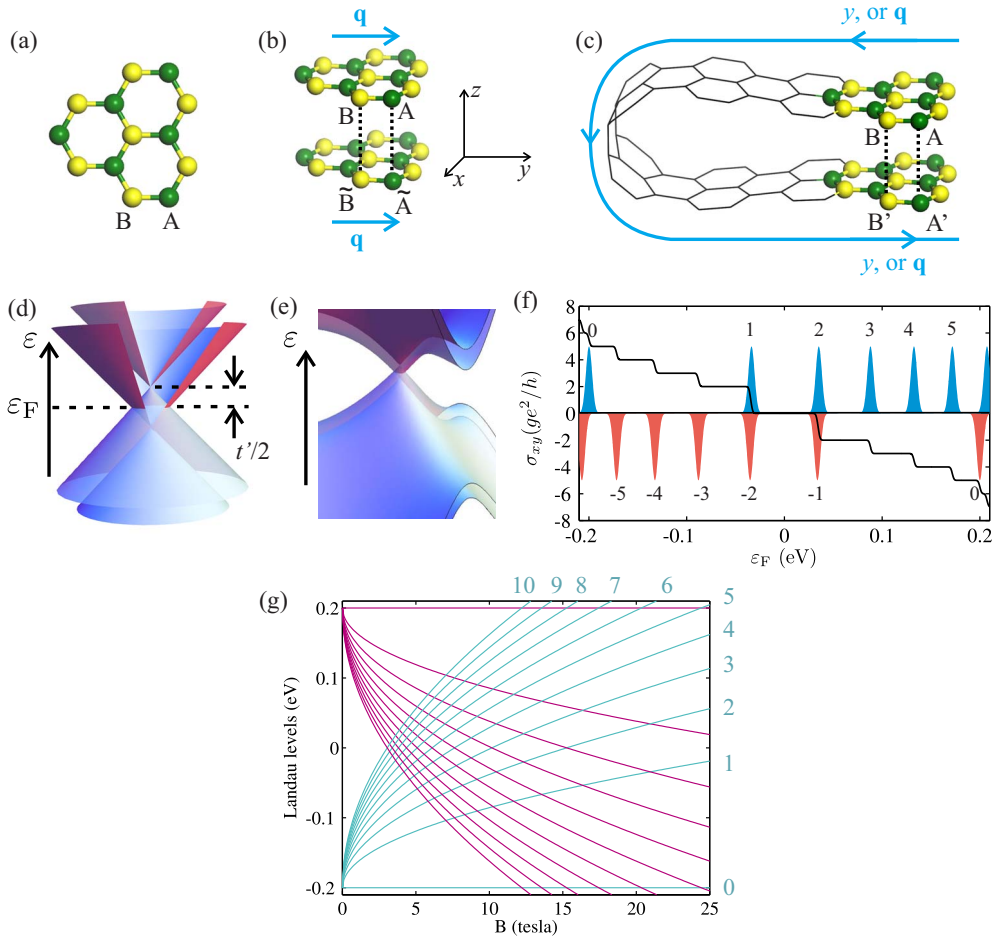


FIG. 3. (Color online) Tight-binding formulation of the electronic structure of graphene and BLE structures. (a) In a single layer graphene, there are two sublattices, designated A (green) and B (yellow). In each of the sublattices, all carbon atoms are related by walks prescribed by the translational symmetry of the underlying hexagonal lattice. (b) The model described in our VP1 (see text). The vertical dotted lines represent the interlayer hopping with *AA* stacking. (c) The model described by our VP2 (see text). The bent honeycomb net of continuous bilayer edge is shown by black lines. (d) The dispersion near the Dirac point calculated from the tight-binding formulation according to our VP1. (e) The DFT-LDA band structure calculated for an extended graphene bilayer with *AA* stacking. (f) A schematic illustration of the quantum Hall effect in *AA*-stacked bilayer, including the DOS of Landau levels (with an arbitrary width) and expected Hall conductivity, for an applied magnetic field with flux density of 21 T (along the $z$ direction). The degeneracy factor, $g$, accounts for intervalley and spin symmetries. (g) Landau levels between $-t'/2$ and $t'/2$ eV as functions of $B$ up to $n=10$, given by $\mathrm{LL}_n = \pm t'/2 \mp 0.0362\sqrt{nB}$ (in eV if $B$ is in teslas). The levels belonging to the lower double cone are labeled.

ter of the curvature and lower on the opposite side. Consequently, a local dipole develops as soon as there is an appreciable curvature in the armchair BLE (point B in Figs. 1 and 2), as the electron density relaxes across the central arc to the roomier side. Then the local dipole moment changes sign at the inflection point at C and does so again when the curve goes through maximum at D. In the case of zigzag BLE, the curvature remains small until ~2.5 Å from the edge. The overall dipole moment densities along the edges, attributable to the bilayer edges, for armchair and zigzag BLEs are calculated to be 1.14 and 0.87 debye/Å, respectively, on par with the rough estimate based on our qualitative model. These extensive spontaneous polarizations, atypical of elemental carbon, can potentially modify the intercalation chemistry and intercalant/adsorbate diffusion kinetics inside the continuous bilayer edges for polar molecules. 1.14 debye/Å (armchair) and 0.87 debye/Å (zigzag) are in fact exceptionally large dipoles. For comparison, $H_2O$ molecule has dipole moment 1.85 debye and CO molecule has dipole moment 0.122 debye.

Many of the most interesting properties of graphene-related materials are derived from their electronic structures. A GML consists of two interpenetrating two-dimensional (2D) triangular sublattices, designated A and B [see Fig. 3(a)]. Following the standard TB formulation,[3,5,8,26–29] there can be two viewpoints regarding the electronic structure of bilayer graphene: one infinite sized and the other finite sized, BLE nanoribbon. In the first viewpoint (VP1), we focus only on the interlayer hopping interaction (with a hopping integral, $t'=0.4$ eV) of two infinite graphene layers with *AA* stacking. As we show in Fig. 3(b), an atom site of the top layer A (B) is coupled with $\tilde{\mathrm{A}}$ ($\tilde{\mathrm{B}}$) of the bottom layer. We designate the graphene lattice sites as A and B and $\tilde{\mathrm{A}}$ and $\tilde{\mathrm{B}}$ for the top and bottom layers, respectively [Fig. 3(a)]. As there are four basis atoms per unit cell. We can represent the

energy by these $4\times4$ blocks because the off-diagonal matrix elements between $|\mathrm{A},kq\rangle$ and $|\tilde{\mathrm{A}},k'q'\rangle$,

$$\langle \mathrm{A},kq|\mathcal{H}|\tilde{\mathrm{A}},k'q'\rangle = \frac{t'}{2}\delta_{k'k}\delta_{q'q} \tag{1}$$

vanishes, except for $k=k'$ and $q=q'$. The Hamiltonian is thus block diagonalizable. Similar relation holds for B and $\tilde{\mathrm{B}}$ sublattices. Arranging the basis as $\{|\mathrm{A},kq\rangle,|\mathrm{B},kq\rangle,|\tilde{\mathrm{B}},kq\rangle,|\tilde{\mathrm{A}},kq\rangle\}$, we have

$$\mathcal{H}_{kq} = \begin{pmatrix} 0 & v_{\mathrm{F}}p & 0 & \tau_\infty \\ v_{\mathrm{F}}p^* & 0 & \tau_\infty & 0 \\ 0 & \tau_\infty^* & 0 & v_{\mathrm{F}}p^* \\ \tau_\infty^* & 0 & v_{\mathrm{F}}p & 0 \end{pmatrix}, \tag{2}$$

where $p=\hbar(k+iq)$ and $\tau_\infty=t'/2$. The four $2\times2$ blocks of Hamiltonian (2) have clear meanings. The two blocks along the principal diagonal describe the bonding within each of the initially isolated graphene layers while the off-diagonal blocks introduce the perturbation of interlayer coupling. Diagonalizing Eq. (2) we obtain the eigen spectrum

$$\varepsilon_k = \pm t'/2 \pm \hbar v_{\mathrm{F}}\sqrt{k^2+q^2}. \tag{3}$$

VP1 gives the infinite-area (bulk) limit of *AA*-stacked bilayer graphene without specifying where the BLEs are. Generally speaking, many single BLEs can connect up and form an arbitrary BLE polygon, with *AA*-stacked bilayer graphene inside or outside of the polygon. Using multiple BLEs, one can get very complex architectures, sometimes resembling a sprawling one-storey building or even more complex topologies.[10,11] The more complex BLE architectures however do not facilitate easy understanding of the contribution due to an individual BLE, in reference to the bulk electronic structure (VP1). In order to study the elementary properties of an individual BLE, we construct a BLE nanoribbon, i.e., two parallel BLEs of the same type separated by a flat bilayer region of width $W$, shown in Fig. 4(a). The BLE nanoribbon is the simplest among all possible BLE architectures that would allow us to extract the elementary properties of a single BLE. All our DFT calculations are actually performed on BLE nanoribbons, illustrated in Fig. 4(a). In our second viewpoint (VP2), then, we try to account for the topological continuity of the honeycomb network around the closed bilayer edges, by starting with a finite BLE nanoribbon, and turn on the interlayer hopping for a subset of A or B sites that correspond to the flat regions in the BLE structures [Fig. 3(c)]. The transverse wave vector, $q$, is now topologically wrapped around the bilayer edge as one travels from the top layer to the bottom layer. Suppose there are $N_y$ A atoms along the $y$ direction. Then the $j$th A atom is paired with $(N_y+1-j)$th A atom, for $1\le j\le N_{c,y}$ (where $N_{c,y}$ is the number of A or B pairs along the $y$ direction). The matrix elements related to the interlayer bonding can then be written, for the A sublattice,

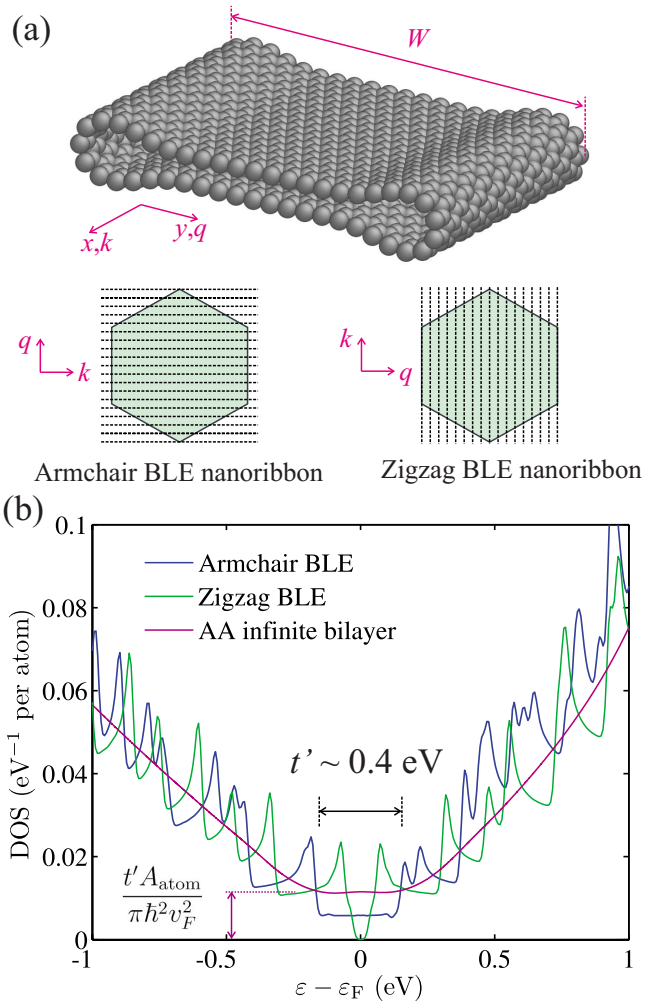


FIG. 4. (Color online) Electronic structure of finite-sized BLE ribbons. (a) The level discretization due to finite size of armchair and zigzag BLE ribbons. The green hexagons are the 1BZ of an extended graphene bilayer. Dashed lines are the loci in the 2D **k** space along which the cuts of the 2D band structures are made. (b) The DFT DOS near the Fermi level of infinite graphene bilayer with *AA* stacking and of the armchair and zigzag BLE nanoribbons, corresponding to our VP1 and VP2, respectively. $A_{\mathrm{atom}}\equiv 3\sqrt{3}b^2/4$ is the area per carbon atom on a monolayer graphene, where $b$ is the C-C bond length.

$$\langle \mathrm{A};kq|\mathcal{H}|\mathrm{A};k'q'\rangle = \frac{t'}{N_y}\delta_{k'k}e^{i\theta(q',N_y)}\sum_{y_n\in\text{pairs}}\exp[-i(q+q')y_n], \tag{4}$$

where $\theta(q',N_y)=(N_y+1)q'h_y$ (where $h_y$ is the separation of neighboring atoms along the $y$ direction). Similar relation holds for interlayer interactions within the B sublattice.

The Hamiltonian derived from Eq. (4) is not strictly block diagonalizable. But the structure of Eq. (4) enables us to make some sensible approximation. The first observation we make is that when $q=-q'$, we have

$$\langle \mathrm{A};kq|\mathcal{H}|\mathrm{A};k'(-q)\rangle = \frac{N_c t'}{N}\delta_{k'k}e^{i\theta}, \tag{5}$$

which are independent of $q,q'$, where $N_c$ is the total number pairs coupled through $t'$ and $N$ is the total number of atoms in the system. On the other hand, when $q \neq -q'$, the *magnitude* of the sum in Eq. (4) becomes

$$\frac{1}{N_y}\left|\sum_{y_n \in \text{pairs}} \exp[-i(q+q')y_n]\right| = \left|\frac{\sin[N_{c,y}h_y(q+q')/2]}{N_y \sin[h_y(q+q')/2]}\right|. \tag{6}$$

For experimentally observed BLEs,[10,11] $N_{c,y} \gg 1$. We observe then from Eq. (6) that the magnitude of an off-diagonal element for $q \neq -q'$ decays rapidly with $|q+q'|$ from $|q+q'|=0$ and is appreciable for $|q+q'| \leq 2\pi/N_{c,y}h_y$. These observations lead to our assumption that the Hamiltonian of VP2 is quasiblock diagonalizable and the only important blocks of the Hamiltonian are those which embed the coupling between $q$ and $-q$ waves. Arranging the basis as $\{|\mathrm{A},q\rangle,|\mathrm{B},q\rangle,|\mathrm{B},-q\rangle,|\mathrm{A},-q\rangle\}$, we then have

$$\mathcal{H}_{kq} = \begin{pmatrix} V & v_\mathrm{F}p & 0 & \tau_N \\ v_\mathrm{F}p^* & V & \tau_N & 0 \\ 0 & \tau_N^* & V & v_\mathrm{F}p^* \\ \tau_N^* & 0 & v_\mathrm{F}p & V \end{pmatrix}, \tag{7}$$

which leads to the eigen energy spectrum

$$\varepsilon_k = V \pm t'N_c/N \pm \hbar v_\mathrm{F}\sqrt{k^2+q^2}. \tag{8}$$

It can be shown that the diagonal terms $V \sim 1/N$, which produces a negligible shift of all bands. When the system is infinitely large along the $y$ direction (and $N_c/N \to 1/2$), Eq. (8) converges to the dispersion of the model in VP1.

The dispersion derived from VP1 [$V=0$ and $N_c/N=1/2$ in Eq. (3)] immediately reveals interesting electronic features of these bilayer graphene with *AA* stacking. The dispersion at the Dirac points in this limit is depicted in Fig. 3(d). The initially double-cone dispersion of a GML is split into a pair, symmetrical about the Fermi level, with an energy offset $t'$. The intersection of these double cones is a contour, which is a Fermi circle for the neutral system centered at $K$. When the system is doped,[7] the Fermi level will be shifted away from the band center by an energy $\varepsilon_\mathrm{F}$. Consequently, the Fermi-surface bifurcates into double circles. We also note that the linearized tight-binding dispersion near $K$ compares quite well with that from DFT-LDA calculation [see Figs. 3(d) and 3(e)]. Notable differences are the trigonal warping[30] and absence of electron-hole symmetry in the DFT spectrum, which are not expected to be captured by the nearest-neighbor-only TB model.

The twinned double-cone spectrum leads to interesting QHE for these bilayers. When we impose the Onsager-Lifshitz quantization[31,32] on the **k**-space area of the cyclotron orbits, we have

$$\mathcal{A}_n = \mathcal{A}_o(n+\gamma), \tag{9}$$

where $\gamma = 1/2 - \Phi_B/2\pi$ (where $\Phi_B$ is the Berry phase). The area quantum is $\mathcal{A}_o = 2\pi eB/\hbar$, where $B$ is the magnetic-flux density. Here, each of the double cones preserves the Berry phase [which can be readily calculated from the eigenvectors of Hamiltonian (2)], $\Phi_B = \pm\pi$, of a GML, entailing each a QHE sequence, $\ldots,-2,-1,0,1,2,\ldots$.

Experimentally, the key variable is the number of charge carriers per unit area of graphene, $C = 2t'\varepsilon_\mathrm{F}/\pi\hbar^2 v_\mathrm{F}^2$, for a small amount of chemical or field doping such that $|\varepsilon_\mathrm{F}| < t'/2$, where degeneracy of $K$ and $K'$ is considered. This linear dependence of $C$ on $\varepsilon_\mathrm{F}$ is starkly different from GML (Ref. 1) or AB bilayer[6] but reminiscent of the 2D electron gas with quadratic band edges in a semiconductor. On the other hand, the semiclassical cyclotron orbit area, $\mathcal{A}$ depends linearly on $(\varepsilon_\mathrm{F} \pm t'/2)^2$. As a result of the different scaling of $C$ and $\mathcal{A}_n$ with $\varepsilon_\mathrm{F}$, there is a *variable* effective energy shift between the two QHE sequences that depends on both $\varepsilon_\mathrm{F}$ and $B$.

Such nonalignment of the QHE sequences with varying energy shifts then represents an interesting case for the QHE experiment. As we show in Fig. 3(f), the locations of quantized orbits of the two QHE sequences in general do not overlap as the dopant concentration varies. Therefore, general quantized increment of the Hall conductivity ($\sigma_{xy}$) is by and large preserved. However, there can be "accidental" near degeneracy of the Landau orbits [see Fig. 3(f)]. The anomalous resonance between the Landau levels from the two double cones will then lead to double steps in the $\sigma_{xy}$, such as the $(1,-2)$ and $(2,-1)$ pairs in Fig. 3(f). Evidently, the location of these resonance steps can be tuned by changing the magnetic field that determines the area quantum of cyclotron. As we show in Fig. 3(g). We see that with certain magnetic field strengths the resonance happens between an even-numbered Landau level and an odd-numbered Landau level from the two double-cone spectra, which leads to two resonance Hall conductivity steps at nonzero doping. On the other hand, with some magnetic field strengths, the Landau levels intersect at zero Fermi level, which should lead to a single resonance Hall conductivity step at the zero level.

When the system is finite, the continuity at the BLE must be taken into account by adopting our VP2. In addition, the band dispersion becomes discrete due to the finite-size effect, in the same way as in graphene nanoribbons.[28] The continuous cone surfaces of VP1 are now sectioned into "noodles" along equispaced lines in the 2D **k** space in VP2 [see Fig. 4(a)]. It is clear from Eq. (8) that details of electronic structure is tunable by virtue of changing the extent of the flat region of the BLE structures, when the size of a BLE structure is finite as described by our VP2.

In Fig. 4(b) we show the DFT density of states (DOS, on a per atom basis) of infinite graphene bilayer with *AA* stacking and of the armchair and zigzag BLE ribbons (two identical BLEs sandwiching a flat graphene bilayer region of width $W$), highlighting further the difference between our VP1 and VP2. The DOS of an infinite bilayer is flat in the energy window between $\pm t'/2$ from the Fermi level, as expected. Outside this range, the DOS is roughly linear in $\varepsilon$ with a finite slope. For the finite armchair BLE ribbon, the DOS in the vicinity of Fermi level is again flat but is smaller than the former since only a subset of the states on the cone are now populated here. Outside this window, the DOS of armchair BLE shows roughly overall trend as the infinite

bilayer but it also shows sharp peaks, which are one-dimensional van Hove singularities. These singular peaks arise from the smooth band edges of the noodles sectioned from the cone off its principal axes. The finite zigzag BLE nanoribbon, however, has features in the DFT DOS [Fig. 4(b)] not accounted for by the approximate TB model; i.e., the dispersion near the Fermi level has quadratic branches, both with small gaps, resulting in a small overall gap in the DOS. By numerically solving the full TB Hamiltonian, we can obtain the gap for zigzag nanoribbons as in DFT calculations. The appearance of gap is interesting for logic applications due to the possibility of gated switching.

In closing, we note that the magnetic length of magneto-oscillation is $l_B=\sqrt{\hbar/eB}=5.6$ nm for $B=21$ T (well in the range of fields applied in typical QHE experiments). The largest experimentally prepared BLEs may have a (folded) width of $\sim$20 nm,[10] which is comfortably larger than the magnetic length mentioned. As the proposed resonance between the two QHE sequences can be straightforwardly controlled by adjusting the applied magnetic field, this property will also offer extra tunability of the electronic characteristics of the BLE based devices, which is not possible at all in graphene monolayer or graphene bilayer with *AB* stacking.

J.F., L.Q., and J.L. would like to acknowledge the support by NSF under Grant No. CMMI-0728069, Honda Research Institute USA, DOE under Grant No. DOE-DE-FG02-06ER46330, AFOSR, and ONR under Grant No. N00014-05-1-0504. This work was performed, in part, at the Center for Integrated Nanotechnologies, a U.S. Department of Energy, Office of Basic Energy Sciences user facility. Sandia National Laboratories is a multiprogram laboratory operated by Sandia Corporation, a Lockheed-Martin Co., for the U.S. Department of Energy under Contract No. DE-AC04-94AL85000.

*liju@seas.upenn.edu

[1] K. S. Novoselov, A. K. Geim, S. V. Morozov, D. Jiang, Y. Zhang, S. V. Dubonos, I. V. Grigorieva, and A. A. Firsov, Science **306**, 666 (2004).
[2] Y. Zhang, Y.-W. Tan, H. L. Stormer, and P. Kim, Nature (London) **438**, 201 (2005).
[3] F. D. M. Haldane, Phys. Rev. Lett. **61**, 2015 (1988).
[4] Y. Zheng and T. Ando, Phys. Rev. B **65**, 245420 (2002).
[5] A. H. Castro Neto, F. Guinea, N. M. R. Peres, K. S. Novoselov, and A. K. Geim, Rev. Mod. Phys. **81**, 109 (2009).
[6] K. S. Novoselov, E. McCann, S. V. Morozov, V. I. Fal'ko, M. I. Katsnelson, U. Zeitler, D. Jiang, F. Schedin, and A. K. Geim, Nat. Phys. **2**, 177 (2006).
[7] T. Ohta, A. Bostwick, T. Seyller, K. Horn, and E. Rotenberg, Science **313**, 951 (2006).
[8] E. McCann and V. I. Fal'ko, Phys. Rev. Lett. **96**, 086805 (2006).
[9] S. V. Rotkin and Y. Gogotsi, Mater. Res. Innovations **5**, 191 (2002).
[10] Z. Liu, K. Suenaga, P. J. F. Harris, and S. Iijima, Phys. Rev. Lett. **102**, 015501 (2009).
[11] J. Y. Huang, F. Ding, P. Lu, L. Qi, and J. Li, Proc. Natl. Acad. Sci. U.S.A. **106**, 10103 (2009).
[12] P. E. Lammert, P. Zhang, and V. H. Crespi, Phys. Rev. Lett. **84**, 2453 (2000).
[13] W. Kohn and L. J. Sham, Phys. Rev. **140**, A1133 (1965).
[14] L. Qi, J. Y. Huang, J. Feng, and J. Li (unpublished).
[15] C. Herring, Phys. Rev. **82**, 87 (1951).
[16] H. Mori, S. Ogata, J. Li, S. Akita, and Y. Nakayama, Phys. Rev. B **76**, 165405 (2007).
[17] P. Koskinen, S. Malola, and H. Hakkinen, Phys. Rev. Lett. **101**, 115502 (2008).
[18] D. M. Ceperley and B. J. Alder, Phys. Rev. Lett. **45**, 566 (1980).
[19] L. A. Girifalco and M. Hodak, Phys. Rev. B **65**, 125404 (2002).
[20] G. Kresse and J. Hafner, Phys. Rev. B **47**, 558 (1993).
[21] D. Vanderbilt, Phys. Rev. B **41**, 7892 (1990).
[22] P. E. Blöchl, Phys. Rev. B **50**, 17953 (1994).
[23] G. Kresse and D. Joubert, Phys. Rev. B **59**, 1758 (1999).
[24] Q. Lu, M. Arroyo, and R. Huang, J. Phys. D **42**, 102002 (2009).
[25] T. Dumitrică, C. M. Landis, and B. I. Yakobson, Chem. Phys. Lett. **360**, 182 (2002).
[26] J.-C. Charlier, J.-P. Michenaud, X. Gonze, and J.-P. Vigneron, Phys. Rev. B **44**, 13237 (1991).
[27] J.-C. Charlier, J.-P. Michenaud, and X. Gonze, Phys. Rev. B **46**, 4531 (1992).
[28] J.-C. Charlier, X. Blase, and S. Roche, Rev. Mod. Phys. **79**, 677 (2007).
[29] A. Cresti, N. Nemec, B. Biel, G. Niebler, F. Trozon, G. Cuniberti, and S. Roche, Nano Res. **1**, 361 (2008).
[30] M. S. Dresselhaus and G. Dresselhaus, Adv. Phys. **51**, 1 (2002).
[31] L. Onsager, Philos. Mag. **43**, 1006 (1952).
[32] A. M. Kosevich and I. M. Lifshitz, Sov. Phys. JETP **2**, 646 (1956).